veins, the sample completely liquifies. Therefore, the corresponding equation for f_l is

$$f_l = \frac{B}{(t - c_0/f_l)^2}\,, \tag{37}$$

which has a simple analytical solution. Again, we examine the leading order contributions in the limiting cases $t \to 0$ and $t \to \infty$ to find

$$f_l \overset{t\to 0}{\longrightarrow} \frac{B}{t^2} + \frac{2c_0}{t} - \frac{c_0^2}{B} + \mathcal{O}(t) \quad \text{and} \tag{38}$$

$$f_l \overset{t\to \infty}{\longrightarrow} \frac{c_0}{t} + \frac{\sqrt{Bc_0}}{t^{3/2}} + \frac{B}{2t^2} + \mathcal{O}\left(\frac{1}{t^{5/2}}\right)\,, \tag{39}$$

where the latter relation is an extension of Eq. (34) which is undefined in the limit $t \to \infty$ and $A \to 0$.

Non-zero surface charge In the general case with immobile surface charges ($q_s \neq 0$) we solve Eq. (21) numerically. In Fig. 7 we show results for a matrix of fused quartz with a grain size of $R = 500$ μm, which may serve as a model for frozen soils. The surface charge density is chosen to be $q_s = 0.5$ C/m^2 which has the correct order of magnitude for mineral/water interfaces at high pH [10]. The ice which fills the voids of the porous matrix is taken to be polycrystalline with a grain boundary density $\rho_{\rm gb} = 1$ μm^{-1}. A comparison of Eqs. (14) and (15) shows that for the given $\rho_{\rm gb}$ the surface area provided by grain boundaries is by a factor 100 larger than the surface area of the porous matrix. Therefore, we expect the impurity concentration in the sample to be very low when grain boundaries are melted and, according to Eq. (24), the maximal undercooling $\Delta T_{\rm max}$ for which quasi-liquid interfacial water at the grain boundaries is stable should be low. An upper limit for $\Delta T_{\rm max}$ can be calculated by assuming that all the impurities in the sample are located at the premelted grain boundaries. For the values of ρ_0 from Fig. 7 we use $N_i = \rho_0/\rho_{\rm gb}$ to obtain a range $N_i = 0.01 - 0.1$ μmol/m^2 and, with the aid of Eq. (24) this corresponds to a range in $\Delta T_{\rm max}$ of $0.01 - 0.26$ K. The range of $\Delta T_{\rm max}$ uses the Hamaker constant $A_H = 3.3 \times 10^{-22}$ J computed from complete dispersion force theory [6] in the limit of thin layers with the data for the dielectric functions from Elbaum and Schick [11]. Including a typical surface charge density of $q_s = 0.01$ C/m^2 for the grain boundary [12] lowers these values to $\Delta T_{\rm max} = 0.01 - 0.20$ K. Hence, the grain boundaries are always collapsed to zero film thickness for the range of ΔT considered in the figure. A prominent feature of $f_l = f_l^{\rm tot}$ with $\rho_0 = 0.01$ mol/m^3 in the fused quartz matrix is the discontinuity at $\Delta T = 22.6$ K where f_l drops by almost an order of magnitude. This is the signature of the collapse of the premelted layer at the ice/fused quartz interface described in detail in Section III A. In the strongly undercooled, layer collapsed system, the only contribution to f_l comes from curvature induced melting; $f_l^{\rm curv} = f_l^{\rm contact} + f_l^{\rm gbmat} + f_l^{\rm veins}$ (cf. Eq. 21), which discontinuously increases at the undercooling where the premelted layer collapses. This is

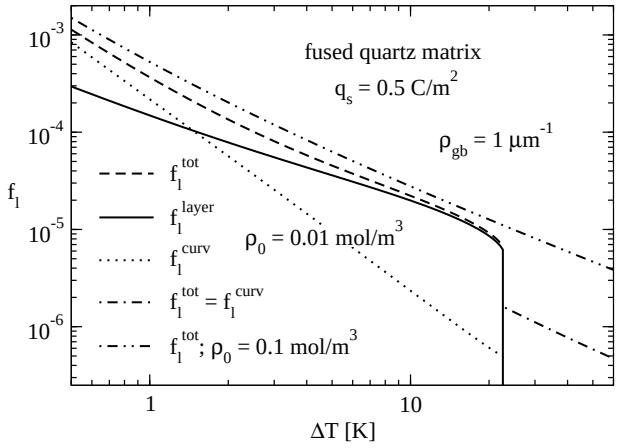

FIG. 7: Liquid fraction f_l for water in a porous matrix of fused quartz with a grain size $R = 500$ μm as a function of the undercooling ΔT. The result for the low impurity density $\rho_0 = 0.01$ mol/m^3 (with respect to the interstitial volume) shows a discontinuity where the quasi-liquid layer between the ice and the matrix collapses. This is accompanied by an increase of the impurity concentration in the remaining (curvature melting induced) liquid which creates a discontinuous increase of $f_l^{\rm curv}$. For the higher impurity density $\rho_0 = 0.1$ mol/m^3 the discontinuity is not visible in the figure because it occurs at large undercooling ($\Delta T \approx 110$ K).

because, due to the efficient rejection of impurities by the ice lattice, the impurity concentration in the remaining liquid increases discontinuously when the liquid layers collapse. At low undercooling curvature melting becomes increasingly important exceeding the contribution from interfacial premelting $f_l^{\rm layer} = f_l^{\rm mat}$. However, at larger undercooling, close to the location of layer collapse, curvature induced melting yields only a minute contribution to f_l. The importance of curvature induced melting at low undercooling is reflected in Eq. (34) where the curvature term B/t^2 dominates for $t \to 0$. In the opposite limit of large undercooling the analytical result Eq. (39) applies. The leading term c_0/t originates from the colligative effect and curvature induced melting enters only through the subdominant term. Hence, for large undercooling the principal contribution to the liquid fraction is the colligative effect. However, liquid water is located in regions of high curvature; contact of matrix spheres, contact lines of grain boundaries and matrix spheres and liquid veins. Figure 7 also shows f_l in the same system with a higher impurity concentration ($\rho_0 = 0.1$ mol/m^3). Here the collapse of the liquid layer is moved to a lower temperature ($\Delta T \approx 110$ K) so that no discontinuity is observed in the range of undercooling considered in the figure.

In Fig. 8 many of the same conditions as in Fig. 7 are considered ($R = 500$ μm, $q_s = 0.5$ C/m^2, $\rho_0 = 0.1$ mol/m^3) the principal difference being that the pore ice is single-crystalline ($\rho_{\rm gb} = 0$). We find that $f_l^{\rm tot}$ in the fused quartz matrix is qualitatively the same as for